Design, Testing of a Prototype Heavy Gas Ring-Imaging Cherenkov (GRINCH) Detector

A thesis submitted in partial fulfillment of the requirement
for the degree of Bachelor of Science with Honors in
Physics from The College of William and Mary

by

Christine McLean

Accepted for Honors
(Honors)

Todd Averett
Advisor: Dr. Todd D. Averett

Dr. Henry Krakauer

Dr. Mark Hinders

Williamsburg, VA
April 2012

"Design, Testing of a Prototype Heavy Gas Ring-Imaging Cherenkov (GRINCH) Detector"

Senior Honors Physics Research

Christine McLean

Dr. Todd Averett, Advisor

Spring 2012

Acknowledgements

I would like to thank everyone who assisted me in this research. I would like to thank Huan Yao for working with me at Jefferson Lab and helping me to understand much of the Cherenkov data acquistion system and data. I would also like to thank everyone else at Jefferson Lab who contributed to this project. Most importantly, I would like to thank my advisor, Dr. Todd Averett, who has advised me in research for most of my undergraduate career and who helped me and motivated me throughout this entire project.

Abstract

The Jefferson Lab experiment E12-06-122 is an ongoing experiment that measures the contribution of quarks to neutron spin. An important part of this experiment is the Cherenkov detector, used to detect electrons scattered off a polarized ^{3}He target. Cherenkov detectors make use of the phenomenon of Cherenkov light, produced when a particle moves faster than the speed of light in the medium through which it travels, to identify particles by velocity. The previous experiment used a Cherenkov detector that did not operate well in the high rate environment in which it operated. The purpose of this experiment is to design and test a prototype for a new Cherenkov detector that will work well in a high rate environment. This report gives an account of the design, setup, and early data analysis of this prototype detector.

Contents

List of Figures

1 Introduction

The purpose of this experiment is to design and test a prototype Cherenkov detector for the Jefferson Lab (JLAB) experiment E12-06-122, which measures the contribution of quarks to neutron spin [1]. The JLAB experiment is aimed at precisely measuring the "virtual photon asymetry A_1^n of the neutron in the Deep Inelastic Scattering (DIS) region using the Hall A polarized ^{3}He target and the Hall A BigBite spectrometer" [2]. Measuring the asymmetry A_1 will give information about the spin carried by the quarks [2]. The JLAB experiment will operate the spectrometer at 30°, where large background rates had been previously observed [3]. It was determined that the previous BigBite Cherenkov detector, used for pion rejection and electron selection did not operate well in high rate environments [1]. Therefore a new, high rate, Cherenkov detector is being constructed to replace the BigBite (BB) Cherenkov detector [1].

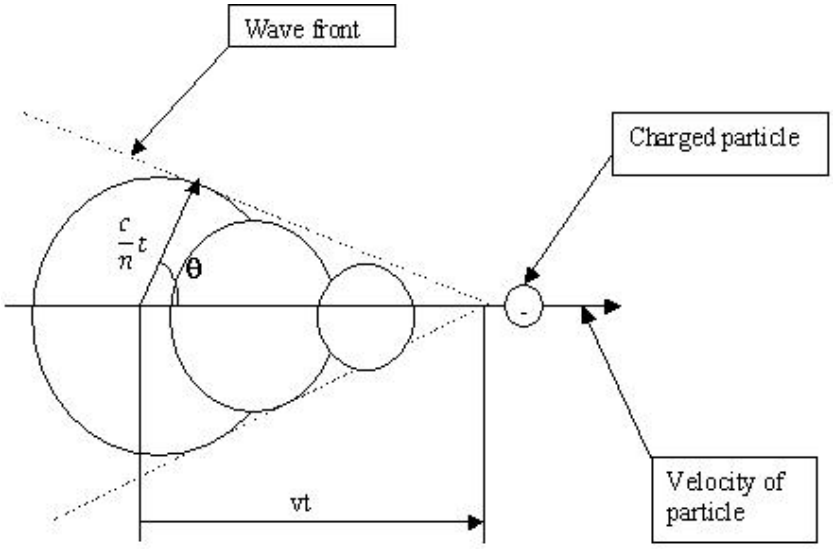

Figure 1: Cherenkov cone [4]

2 Theory

2.1 Cherenkov Radiation

As accelerators have increased in size and energy range, an increasing variety of particle detectors have been used in conjuction with them. One technique in particle identification (PID) has been to make use of Cherenkov radiation. This phenomenon occurs when a particle's velocity exceeds

the speed of light of the medium through which it travels [5]. The effect is equivalent to the shockwave produced when a moving object breaks the sound barrier. However, instead of a cone of sound (mach cone) being produced, during the process of Cherenkov radiation, a cone of light is produced by the particle's motion. This "Cherenkov cone" is defined by the Cherenkov angle θ_c:

$$\cos\theta_c = \frac{1}{\beta n(\omega)} = \frac{1}{(v/c)n(\omega)} \tag{1}$$

where v is the velocity of the particle, c is the speed of light in a vacuum, $n(\omega)$ is the refractive index of the medium, and ω is the frequency of emitted light [6]. Figure 1 depicts this phenomenon. The Cherenkov angle is the angle between the emitted light and the path of the particle [5]. The particle's velocity can be determined by measuring this angle, which is the basic idea behind Cherenkov detectors. It is important to note that the Chrerenkov angle is dependent on the particle's speed and the frequency of emitted light [6]. Figure 2 shows the dependence of the Cherenkov angle θ on $\beta = v/c$ for given values of the index of refraction, n [7].

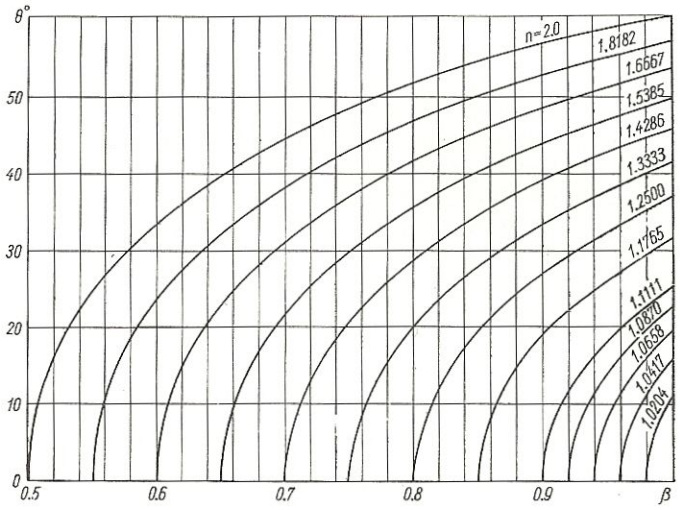

Figure 2: Dependence of Cherenkov angle on particle velocity [7]

Equation 1 describes Cherenkov radiation in an infinite medium [6]. However, the material within all particle detectors has a finite thickness. Using classical electrodynamics, it can be found that the energy radiated per solid angle per unit frequency, by a particle of charge ze moving in a uniform straight line through material of thickness L, is:

$$\frac{d^2E}{d\omega d\Omega} = z^2\frac{\alpha\hbar}{c}n\beta^2\sin^2\theta\left|\frac{\omega L}{2\pi\beta c}\frac{\sin\xi(\theta)}{\xi(\theta)}\right|^2 \tag{2}$$

where n is the refractive index of the medium, α is the fine structure constant, and

$$\xi(\theta) = \frac{\omega L}{2\beta c}(1 - \beta n \cos\theta) \tag{3}$$

The $(\sin\xi/\xi)^2$ term describes Fraunhofer diffraction, which describes diffraction in the far field limit [6]. The inclusion of a diffraction term in Equation 2 indicates that Cherenkov radiation follows a diffraction-like pattern, with the diffraction peak centered about Equation 1. Additionally, if the wavelength of emitted light is small compared to L, the $\sin\xi/\xi$ term becomes the delta function $\delta(1 - \beta n \cos\theta)$ [6]. This leads to an emission pattern following Equation 1, as expected [6].

Integrating Equation 2 over the solid angle gives:

$$-\frac{dE}{d\omega} = z^2 \frac{\alpha\hbar}{c} \omega L \sin^2\theta_c \tag{4}$$

Then, to obtain energy emitted per unit path length, Equation 4 is divided by and then integrated over frequencies which satisfy the Cherenkov threshold condition ($v > c/n(\omega)$), the velocity required to produce Cherenkov radiation) [6]:

$$-\frac{dE}{dx} = z^2 \frac{\alpha\hbar}{c} \int \omega d\omega \sin^2\theta_c = z^2 \frac{\alpha\hbar}{c} \int \omega d\omega \left(1 - \frac{1}{\beta^2 n^2(\omega)}\right) \tag{5}$$

where L is assumed to be larged compared to the wavelength of the emitted light [6].

2.2 Cherenkov Detectors

Cherenkov detectors generally use the threshold condition and the relationship between Cherenkov angle and particle velocity to accurately measure particles' velocity and identify them [6]. One factor of interest to the design of a Cherenkov detector is the number of photons emitted by a particle traversing a certain length of a given medium [6]. This is found by dividing Equation 4 by L and $\hbar\omega$, which gives the number of photons emitted per unit length of the medium per unit frequency [6]:

$$\frac{d^2N}{d\omega dx} = \frac{z^2\alpha}{c} \sin^2\theta_c = \frac{z^2\alpha}{c} \left(1 - \frac{1}{\beta^2 n^2(\omega)}\right) \tag{6}$$

This can also be written in terms of wavelength [6]:

$$\frac{d^2N}{d\lambda dx} = \frac{2\pi z^2\alpha}{\lambda^2} \left(1 - \frac{1}{\beta^2 n^2(\lambda)}\right) \tag{7}$$

In most Cherenkov detectors, the radiation is detected by photomultiplier tubes (PMT's), which generate an electrical current from incident photons [6]. Usually, they are sensitive within the range of 250 nm to 700nm [6]. Equation 7 can be integrated over these limits to find [6]:

$$\frac{dN}{dx} = 2\pi z^2 \alpha \sin^2 \theta_c \int_{\lambda_1}^{\lambda_2} \frac{d\lambda}{\lambda^2} = 475 z^2 \sin^2 \theta_c \text{ photons/cm} \tag{8}$$

This is not a large number, so the detector must be designed to handle smaller signals. Figure 3 shows Cherenkov radiation intensity (in arbitrary units) versus wavelength. This curve follows Equation 7, with $z = 1$ for a single electron; $n = 1.000449$ for $C0_2$, the gas used in the experiment; and $\beta = 0.99956$, which is greater that 0.99955 as required by the Cherenkov threshold condition. The radiation intensity works well with PMTs sensitive in the previously mentioned range.

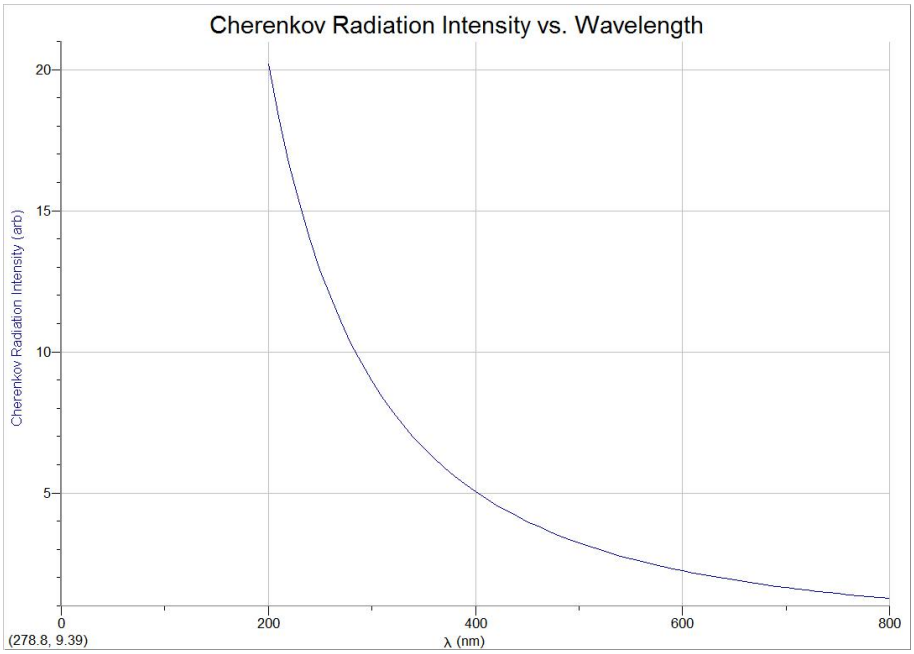

Figure 3: Cherenkov radiation spectrum

All Cherenkov detectors contain a specific amount of material with refractive index n, through which particles travel and emit Cherenkov light. For small θ_c, this radiation can be focused with a spherical mirror of radius R onto a point [9]. Due to the azimuthal symmetry of the Cherenkov cone about the particle trajectory, the focal point of the light is a ring of radius r [9]:

$$r = \frac{R}{2} \tan \theta_c \tag{9}$$

In ring-imaging Cherenkov detectors, this light is focused onto an array of photomultiplier tubes

(PMT's), the data from which can be used to measure r, and therefore v [9]. However, the detector in this experiment is a threshold detector, which will separate the velocities of the particles by using a medium with an appropriate index of refraction so that electrons, but not pions, will produce Cherenkov radiation [3].

The method of using the threshold condition of Cherenkov radiation to separate particles can be done in gases whose indices of refraction are close to 1. Figure 4 lists the indices of refraction of several gases at STP, with $\lambda = 589.3$ nm, as well as the threshold velocities [8]. The gas used in this experiment is $C0_2$, though eventually C_4F_8O will be used, once a supplier can be located. For particles traveling with a momentum of 1000 MeV/c, the thresholds in $C0_2$ are 17.03 MeV for electrons and 4652.81 MeV for pions, which is a reasonable difference.

Gas	Chemical formula	n at $\lambda = 5893$ Å	Threshold velocity
Helium	He	1.000035	0.999965
Neon	Ne	1.000067	0.999933
Hydrogen	H_2	1.000138	0.999862
Argon	Ar	1.000283	0.999716
Air	—	1.000293	0.999707
Carbon dioxide	CO_2	1.000449*	0.999551
Acetylene	C_2H_2	1.000610	0.999390
Ethylene	C_2H_4	1.000696	0.999304
Ethane	C_2H_6	1.000706	0.999294
Freon-13	$CClF_3$	1.000782	0.999219
Propane	C_3H_8	1.001005	0.998996
Freon-12	CCl_2F_2	1.001150**	0.998851
Pentane	C_5H_{10}	1.00177	0.998233

* At $\lambda = 5791$ Å.
** At $\lambda = 5461$ Å.

Figure 4: Indices of refraction and threshold velocities of different gases [8]

As seen in the table, these gases have very high thresholds, so the gas in a Cherenkov detector generally needs to be under pressure [8]. The refractive index of gas as a function of gas density ρ (and therefore, the pressure p) is given by the Lorentz-Lorentz law [8]:

$$\frac{n^2 - 1}{n^2 + 2} \cdot \frac{1}{\rho} = \text{const} \tag{10}$$

where the density ρ is related to the pressure p by [8]:

$$\rho = \frac{p\mu}{RT} \tag{11}$$

where p is the gas pressure, μ is the gas's mass, T is the temperature, and R is the ideal gas constant. For low pressures, such as in this experiment, it can be assumed that $n(p)$ is a linear function [8]. Therefore, gas Cherenkov detectors are quite useful in that the pressure (and therefore refractive index) of the contained gas can by varied, thereby varying the particle detection threshold over a reasonably large velocity range [8]. Even with added pressure, Cherenkov radiation intensity is rather low in gas, so the detectors must have a relatively long path length to get enough detectable radiation [8].

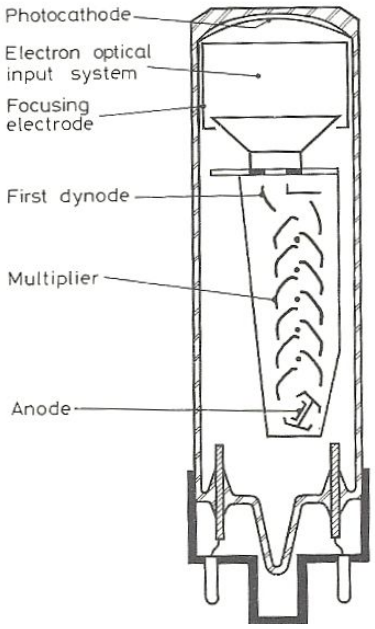

Figure 5: Photomultiplier tube schematic diagram

2.3 Photomultiplier Tubes

Photomultiplier tubes (PMT's) are devices that convert light into a measurable electric current [6]. Figure 5 illustrates the schematics of a typical PMT [6]. The top face contains a photosensitive cathode followed by an electron collection mechanism, an electron multiplier system (also known as the dynode string), and then an anode from which signal is taken [6]. Usually, all parts are contained within an evacuated glass tube [6].

To operate a PMT, a high voltage is applied to the anode, with the cathode at ground, so that

a potential "ladder" is constructed along the length of the cathode-dynode-anode system [6]. When an incident electron hits the photocathode, one or more electrons are ejected due to the photoelectric effect [6]. Due to the applied voltage and the focusing electrode, the electrons are accelerated and directed toward the first dynode [6]. Upon striking, the electron transfer some of their energy to the dynode electrons, which causes the emission of secondary electrons [6]. These electrons are, in turn, accelerated toward the next dynode where more electrons are emitted and accelerated, causing an electron cascade [6]. At the anode, the cascade is collected as a current, which can be amplified and analyzed [6]. Generally, the dynode and cathode systems are assumed to be linear, so the anode current is directly proportional to the number of photons incident on the cathode [6].

As previoulsy mentioned, the photocathode utilizes the photoelectric effect to convert incident photons into a current of electrons [6]. To increase the transmitted light, a layer of photosensitive material is applied to the inside of the PMT window (the top of Figure 5), usually made of quartz or glass [6]. The photoelectric effect is described by the formula:

$$E = h\nu - \phi \tag{12}$$

where E is the emitted electron's kinetic energy, ν is the frequency of the incident light, and ϕ is the work function [6]. Due to the work function, a minimum frequency is required for this phenomenon to take place [6]. However, even above this required frequency, there is nowhere near 100% probability for the photoelectric effect to occur [6]. The efficiency of this process varies with the frequency of the light and the material used. The total spectral response is known as the "quantum efficiency", QE(λ), which is the probability that a photon incident on the cathode converts one or more photoelectrons. Figure 6 shows the quantum efficiency versus wavelength (curve B) for the PMT's used in this experiment [10]. As in most today, these PMT's have a photocathode coating made up of semiconductor materials, which have low work functions compared to metals and have much higher quantum efficiencies [6].

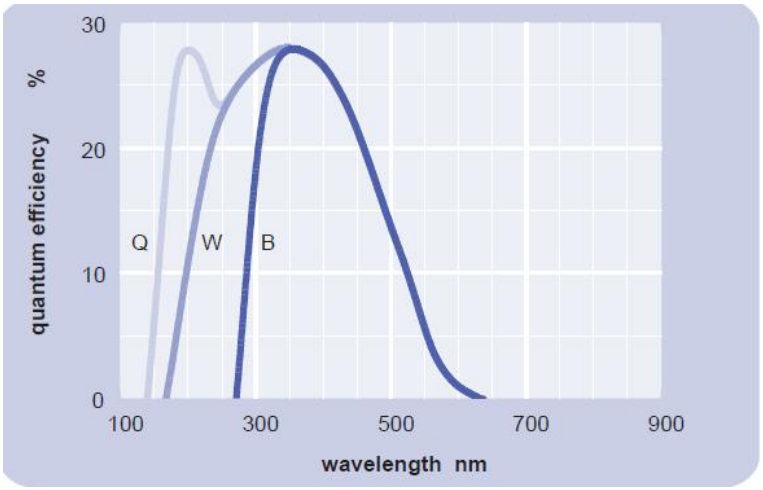

Figure 6: PMT quatum efficiency [10]

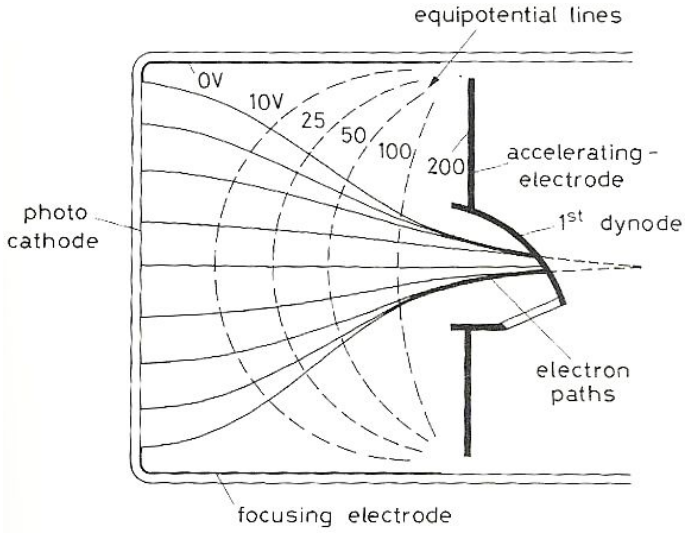

Figure 7: PMT electron-input system [6]

After the electrons are emitted from the photocathode, they are collected and focused onto the first part of the electron multiplier system [6]. This process is acheived through the application of a suitable electric field [6]. Figure 7 illustrates a typical electron-optical input apparatus [6]. In this setup, the accelerating electrode and first dynode are at the same potential and are used along with a focusing electrode on the side of the tube [6]. Equipotential lines and possible electron paths are also shown [6]. No matter the design, there are two important characteristics that need to be met by this system. One, collection efficieny must be as high as possible, i.e. regardless of point of origin on the photocathode, as many emitted electrons as possible must reach the dynodes [6]. Two, of particular importance for detectors that rely on timing, the

electron travel time from the cathode to the first dynode should be independent of the emission point, or at least as independent as possible [6].

In the electron-multiplier part of the PMT, the weak initial photocurrent is amplified using a series of dynodes to produce a measurable current at the PMT anode [6]. The gain of each dynode is called the "secondary emission factor, δ" [6]. The secondary emission process is similar to the initial photoelectric emission except that the incedent photon is now replaced by electrons [6]. When an incident electron strikes a dynode, energy is directly transferred to the electrons in the dynode, causing many secondary electrons to escape the dynode material [6]. Since a constant electric field must be maintained between dynodes in order to move the electrons along the device, the dynode material must contain conductive material [6]. Commonly, an alloy of an alkali (low work function) and a more noble metal is used for this material [6]. Ideally, these alloys have certain characteristics: high δ, stability of emission under high currents, and low noise [6]. Usually PMT's have 10 - 14 stages, with total gain around 10^7.

Theoretically, all fixed energy electrons passing through the dynode system should experience constant gain [6]. However, this is not really possible, since the secondary emission process is a statistical one [6]. Therefore, fluctuations in gain occur, because single electrons of the same energy traversing the dynode system will cause different numbers of secondary electrons to be emitted [6]. A measure of the extent of these fluctuations is given by the"single electron spectrum," the spectrum of PMT output pulses caused by the entry of single electrons into the electron-multiplier system [6]. In practice, this response behavior of the multiplier can be measuring by shining a weak light source on the PMT [6]. Due to the statistical fluctuations, the output pulse shapes will usually be different for the different single-electron events [6]. A new pulse with an amplitude proportional to the total charge can be obtained by integrating each current pulse, and therefore the gain for each electron pulse can also be obtained [6]. Figure 8 shows some single-electron spectra for a linear-focused PMT, the type used in the current experiment [6]. The "b" factor is "the RMS deviation from perfect uniformity of the secondary emission factor over the surface of the dynode" [6]. This kind of PMT has relatively minimal fluctuations in peak height due to a geometry that produces well-focused electrons [6].

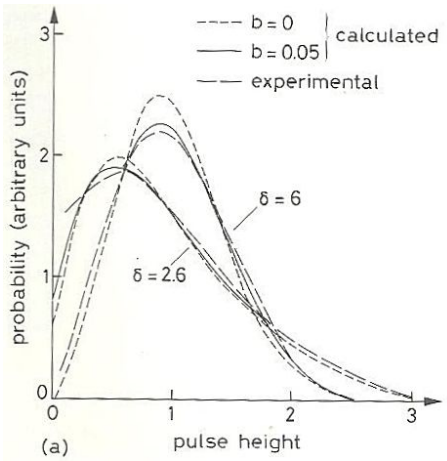

Figure 8: PMT single-electron spectrum [6]

The overall gain of a PMT is dependent on the number of dynodes and the secondary emission factor δ, which depends on the initial electron's energy [6]. In the dynode chain, the energy of each set of incident electrons is a function of the potential difference V_d between the dynodes:

$$\delta = KV_d \tag{13}$$

where$K$ is constant [6]. Generally, the voltage is applied equally across all dynodes, so the overall PMT gain is:

$$G = \delta^n = (KV_d)^n \tag{14}$$

where n is the number of stages in the multiplier chain [6].

As previously mentioned, the anode output signal is a charge pulse with a total charge proportional to the number of electrons initially emitted by the photocathode [6]. Therefore, a PMT may be represented as a current generator placed in parallel with a resistor and a capacitor, as shown in Figure 9 [6]. The capacitance, C, and the resistance, R, represent the intrinsic capacitance and resistance of the anode and the rest of the output circuit [6].

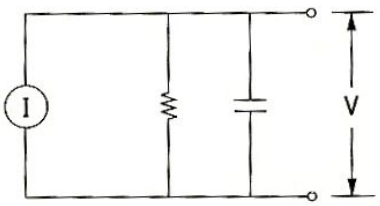

Figure 9: PMT equivalent circuit [6]

This simple schematic can be used to determine the behavior of the signal output from the PMT [6]. If, for example, the input is light from a scintillator, described by exponential decay, the equation for the current from the anode is:

$$I(t) = \frac{GNe}{\tau_s} exp\left(\frac{-t}{\tau_s}\right) \tag{15}$$

where G is the PMT gain, N is the number of photoelectrons emitted by the photocathode, e is electron charge, and τ_s is the scintillator delay constant [6]. This leads to an equation of the form:

$$I(t) = \frac{V}{R} + C\frac{dV}{dt} \tag{16}$$

which has the solution:

$$V(t) = -\frac{GNeR}{\tau - \tau_s}\left[exp\left(-\frac{t}{\tau_s}\right) - exp\left(-\frac{t}{\tau}\right)\right], \text{ if } \tau \neq \tau_s \tag{17}$$

or

$$V(t) = \left(\frac{GNeR}{\tau_s^2}\right) t\left[exp\left(-\frac{t}{\tau_s}\right)\right], \text{ if } \tau = \tau_s \tag{18}$$

where $\tau = RC$ [6]. Figure 10 shows this expression, with different values of τ, plotted with $G = 10^6$, $N = 100$, $C = 10$pF, and $\tau_s = 5$ ns [6].

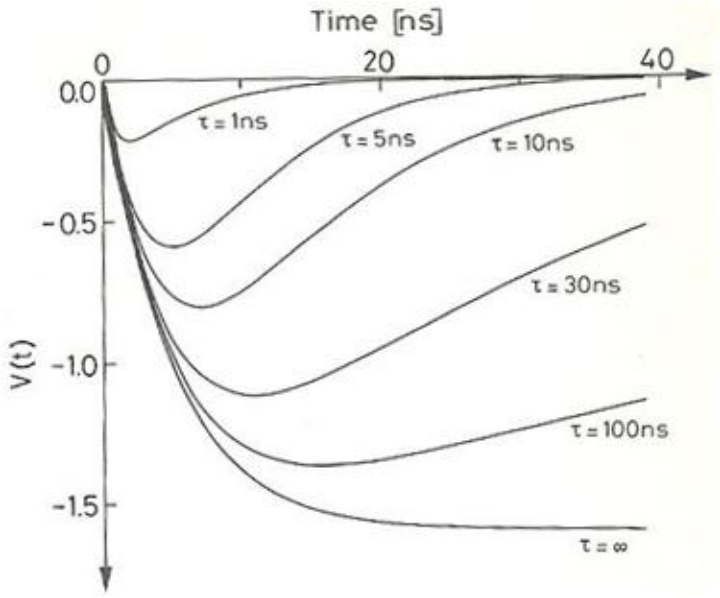

Figure 10: PMT output signals for a range of time constants τ [6]

3 Data Acquisition

Figure 11 shows the complete test stand for the experiment. The parts are as follows: 1 is the GRINCH prototype detector box, 2 is the mirror, 3 is the PMT array, 4 is the path of the electrons, 5 is the Cherenkov light, S_1 - S_4 are scintillator paddles, and P_1 and P_2 are lead glass blocks. The scintillators and lead glass blocks each have one PMT attached to them.

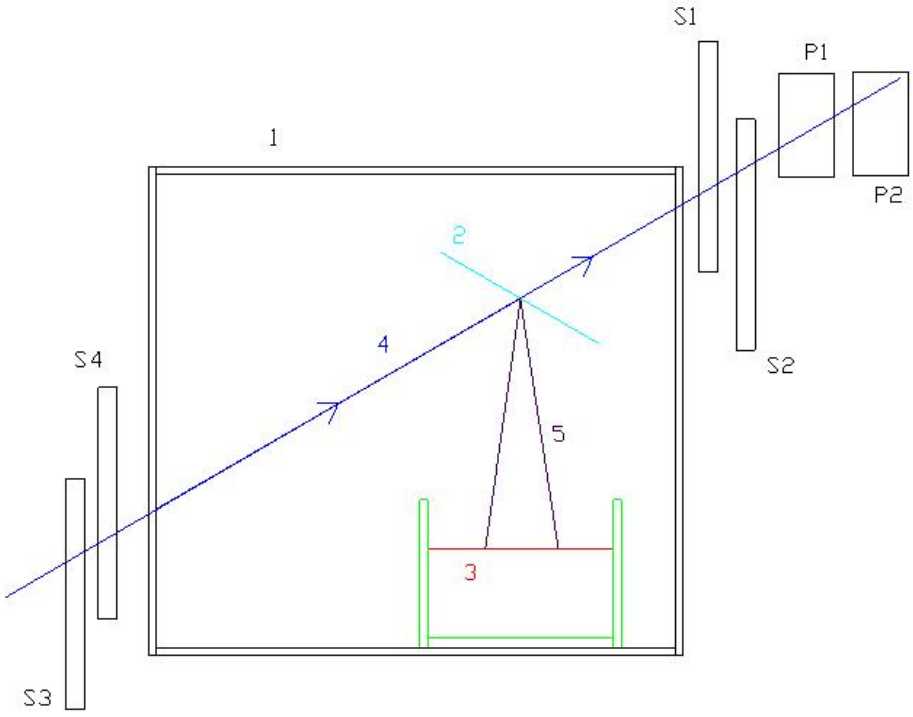

Figure 11: Prototype Cherenkov detector setup

In this data acquisition (DAQ) system, three scintillator signals are required to arrive at the same time, which causes a trigger. If this happens, the trigger signals the system to read out all the PMT's, including those of the scintillators and the lead glass blocks, through TDC's and ADC's. TDC's are time-to-digital converters, which measure a Δt and digitizes this information. In this system, a "good" event should have $\Delta t = t_{\text{PMT}} - t_{\text{trigger}} = \text{const} \pm$ 10ns. ADC's are analog-to-digital converters, which integrate charge, like that of Figure 10, for about 240ns and digitize it. In this experiment, VME TDC's, preceded by discriminators, will be used to read the [ADC] signal in a short 10 ns window around a good event [3].

4 Motivation

As previously stated, the goal of the experiment is the design and testing of a prototype Cherenkov detector for the JLAB E12-06-122 experiment. Specifically, it is to create a heavy **G**as **R**ing-**I**magi**N**g **CH**erenkov (**GRINCH**) detector to detect Cherenkov radiation in a high rate environment, using a large array of small diameter PMT's and new timing methods [3]. In this experiment, the BigBite spectrometer is fixed at a scattering angle of 30° with the GRINCH detector right behind it . The purpose of the Cherenkov detector is for PID, specifically of electrons scattered off of a ^{3}He target [3]. After the spectrometer, the Cherenkov detector will only need to separate the electrons from pions with similar momentum, by selecting for velocity [3]. Figure 12 shows the experimental setup.

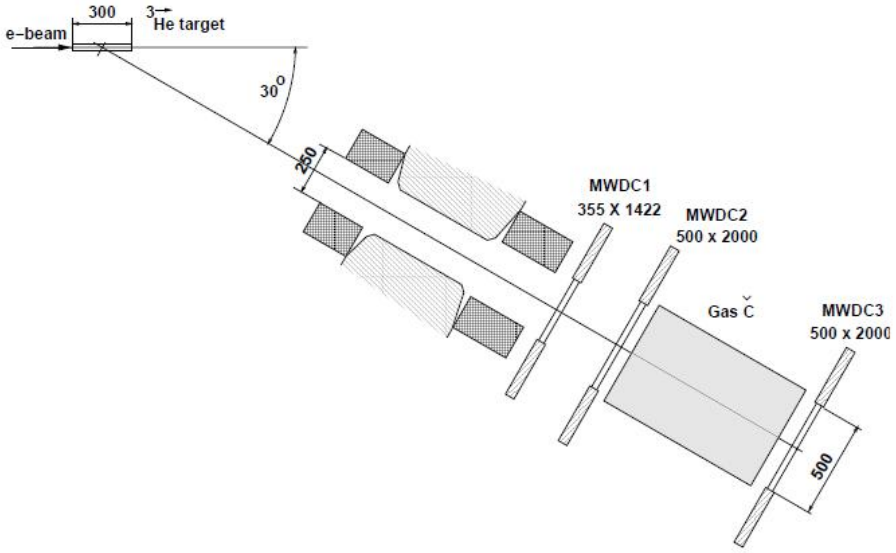

Figure 12: Experimental setup of the target, BigBite spectrometer, and GRINCH detector [2]

In previous experiments, the BB spectrometer was placed at 30° to measure electrons scattered off of the polarized ^{3}He target, with a beam energy of 3-6 GeV and beam current around 12-15 μA [3]. With the experimental setup of the target, spectrometer, and Cherenkov detector, it has been found that when the beam strikes the target cell, a low rate of the"good" electrons is produced. It was found that the backgroud rate was unexpectedly high, especially on the side of the detector nearest to the beamline [3]. It was found that the large diameter (5") PMT's were not suited for a high rate environment [3]. Additionally, the data acquisition ADC method of a long integration (in time) of the PMT current signal picked up additional background [3]. In

the new experiment, the beam current has increased to 30μA and a longer ^{3}He target is being used, so the luminosity seen by the GRINCH detector will increase by a factor of at least 4 [3].

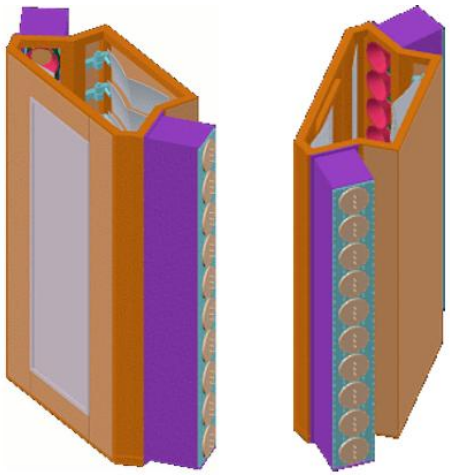

Figure 13: BigBite Cherenkov detector [3]

The previous BB Cherenkov detector contained ten 5" PMT's on each side of the detector, as can be seen in Figure 13. The light was focused onto the PMT's using two mirrors and a Winston Cone (Figure 14). PMT's 1-10 were located on the beamline side of the detector and therefore saw rates an order of magnitude greater than those on the other side [3]. This can be seen clearly in Figure 15 in which the PMT rates are plotted versus discriminator threshold [3]. Predictably, the rates increase when the discriminator threshold is lowered, but are much greater for those PMT's closer to the beamline [3]. Additionally, the BB Cherenkov's PMT's had a glass face that was about 0.5 - 1 cm thick at the thinnest point, causing a high probability of the direct production of more background particles in the glass [3].

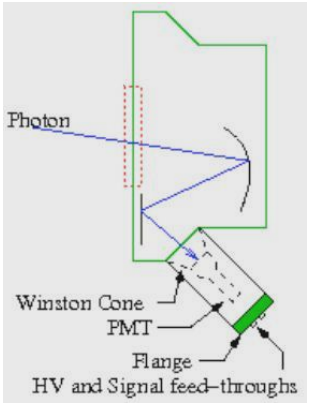

Figure 14: BigBite Cherenkov detector top view[3]

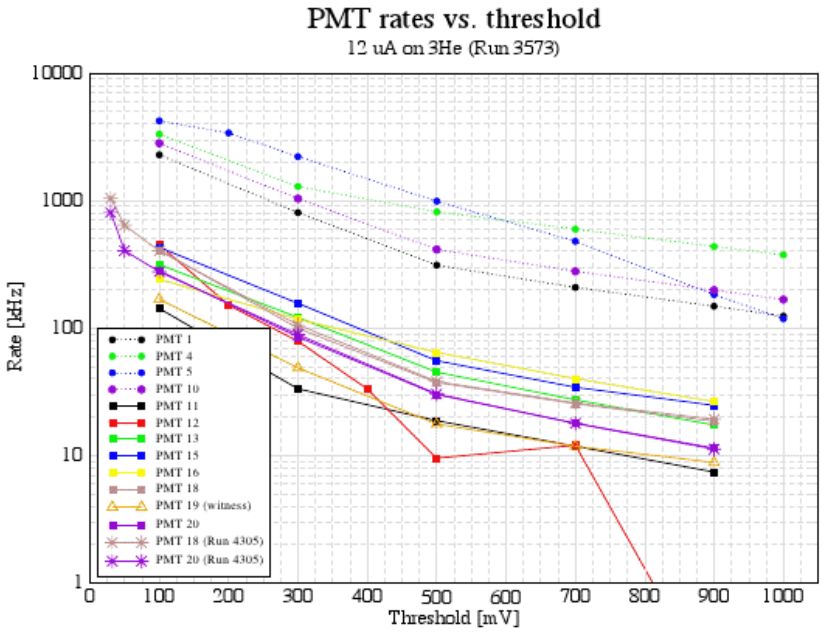

Figure 15: PMT rates versus threshold in previous experiment[3]

The maximum single electron rate for the BB Cherenkov PMT's on the large-angle side, with a threshold of 100mV, was 400 kHz. The GRINCH prototype detector uses 81 29 mm diameter PMT's. Using these photomultiplier tubes, the active area decreases by a factor of $(1.14/5)^2 = 0.052$. Due to increased luminosity, rates will increase by a factor of at least 4, so the rate per tube should be at least 83 kHz [3]. Additionally, if it is true that background was produced in the thick glass of the large PMT faces, the thinner glass of the smaller PMT's should reduce this background [3].

As previously mentioned, most ring-imaging Cherenkov detectors use the ring of light produced in the Cherenkov cone and Equation 9 to determine θ_c and therefore identify the particle velocity and the particle itself [9]. In this case, a spherical mirror is used to focus the light [9]. Since the GRINCH detector is a threshold detector, the ring will be used for timing purposes. The geometry places many more tubes within each Cherenkov detection ring of radius r (Equation 9) than before. With this setup, a "good" event will fire a cluster of PMT's at once. A background event, causing one or two PMT's to fire, can therefore be eliminated, because it will be distinguishable from a good event [3]. Figure 16 shows a sample cluster recorded during calibration (not during this project) of the data taking system. In this array of 64 of phototubes, the green tubes represent the TDC's that fired for each event. Five green tubes in a cluster indi-

cate a "good" event. When the Cherenkov light ring is used in this manner, its radius does not need to be measured, so precise focusing is less vital than for a standard ring-imaging detector. Therefore, a flat mirror is being used in the prototype detector. In the final GRINCH detector, a cylindrical mirror will be used [3].

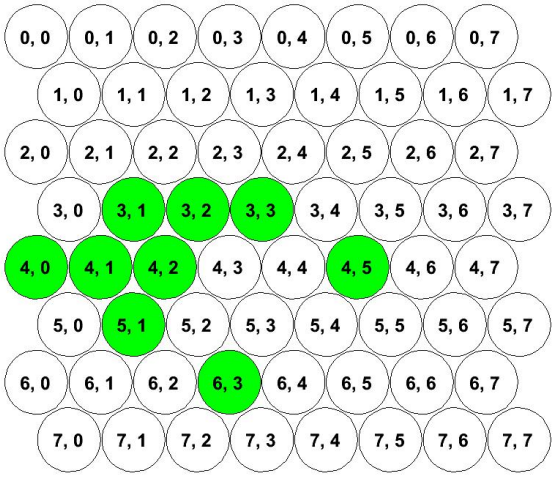

Figure 16: PMT event display

Figure 17 shows one of the PMTs to be used in the GRINCH detector. Some important features to note are that its maximum quantum efficiency is in the 300-450 nm range (Figure 6), which is good for detecting Cherenkov radiation. Additionally, the maximum gain is around 10^7.

Figure 17: Photomultiplier tube

The most important requirements of the GRINCH detector design are: capability to see signal in a high background environment, pion rejection up to a momentum of 3.5 GeV/c, and pion rejection better than 50:1 [3]. Some of the key elements of the new design are as follows. First, the detector will contain a slightly pressurized heavy gas, C_4F_80, which has an index of refraction of 1.00135, though $C0_2$, which has an index of refraction of 1.00049 is currently being used [3]. Second, the path length is to be increased from 40 cm - 70 cm in order to increase the

signal produced [3]. As previously described, a large array of small diameter photomultipliers tubes are to be used to reduce background sensity and (theoretically) reduce the production of background particles in the glass face of the PMT [3]. Additionally, the PMT array is to be located on the large-angle side (farther from the beam) of the BigBite spectrometer, where background rates should be lower [3].

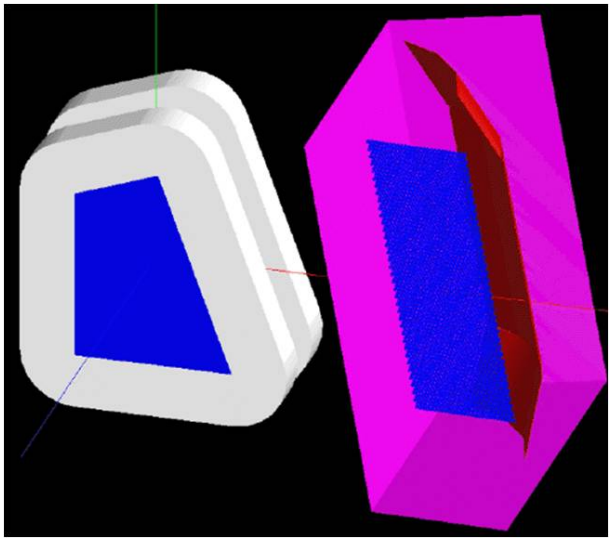

Figure 18: Detector geometry simulation: side view [3]

Figure 18 shows a side-view simulation of the GRINCH detector, which uses 4 cylindrical mirrors to deliver the Cherenkov light to the PMT array, located on the large angle side [3]. The white apparatus is the BigBite Spectrometer, the fuchsia is the GRINCH detector enclosure, the red is the mirrors, and the blue is the PMT array. Figure 19 shows a top-view simulation of the GRINCH detector, where the electrons (red path) travel through the BigBite detector and then enter the blue box of the GRINCH detector. The green is the light given off by the electrons in the detector; this light is focused by the red mirror onto the PMT array. The path length of the electrons is the distance between their point of entry into the detector and their point of impact on the mirror.

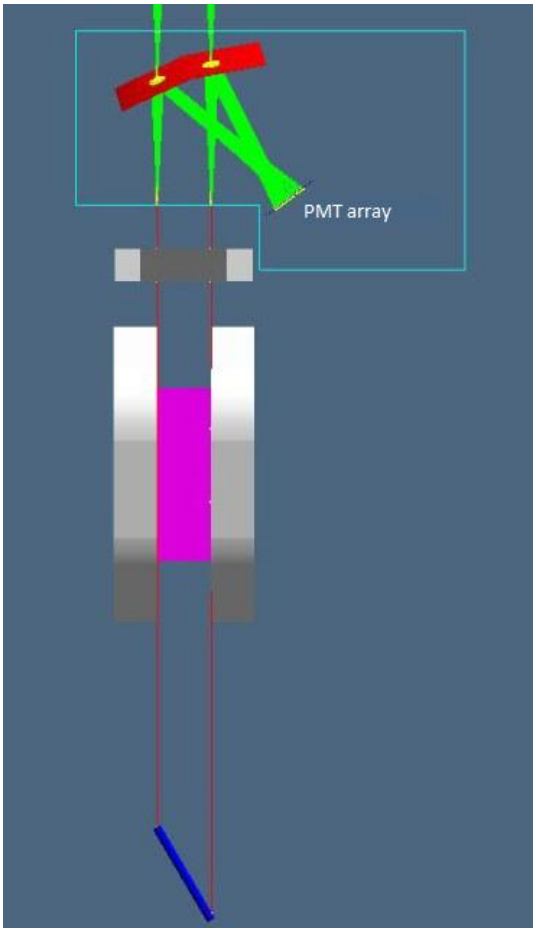

Figure 19: Detectorgeometry simulation: top view [11]

The final important improvement is that the detector readout has been changed from an integrating ADC/QDC method, which uses a long integration (240 ns) of the detector signal and therefore integrates a lot of background noise [3]. As previously mentioned, in the new detector, the data is to be read through VME TDC's, preceded by discriminators, to read the signal in a short timing window around a good event [3]. Therefore noise will be reduced by a reduction in readout time, 10 ns vs. 240 ns, and the detection system should be more suited for a high rate environment [3].

Figures 20 and 21 show example results of a TDC and ADC calibration, respectively. Each histogram corresponds to one phototube in the array and has events on the y-axis. The TDC histograms (Figure 20) show the TDC data (time on x-axis) after the signal triggered the electronics and the TDC started counting. The ADC histograms show integrated charge with energy on the x-axis. The black peak is called the pedestal and is not part of the good data. It happens

for every reading and indicates the integrated signal due to a DC offset or constant background electronics noise. The actual data is shown by the red curve, which was determined by a TDC-based cut, the red lines in Figure 20. The first peak to the right of the pedestal is due to single photo-electron events in the PMT's, while the multi-electron events lie farther right on the graph.

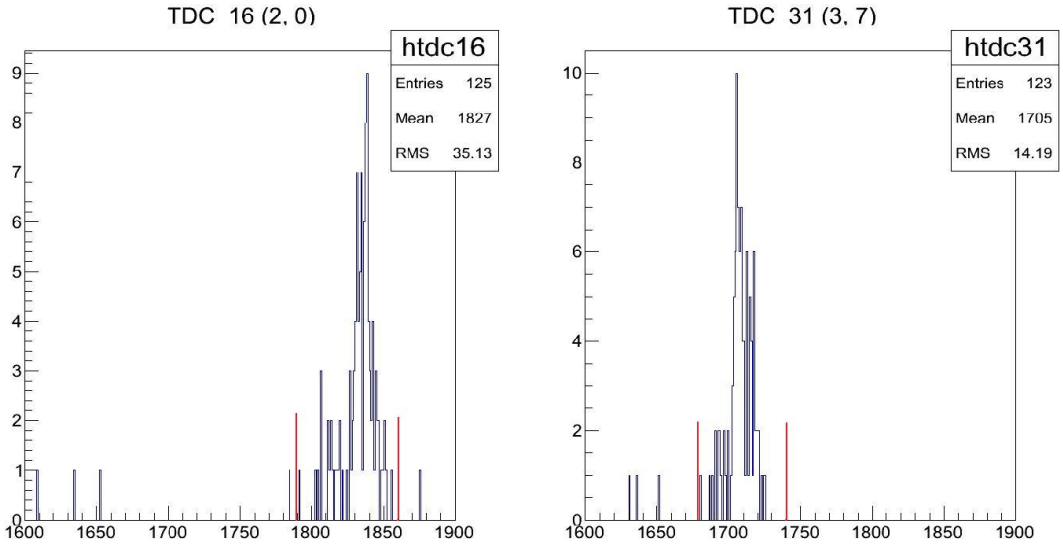

Figure 20: TDC histograms

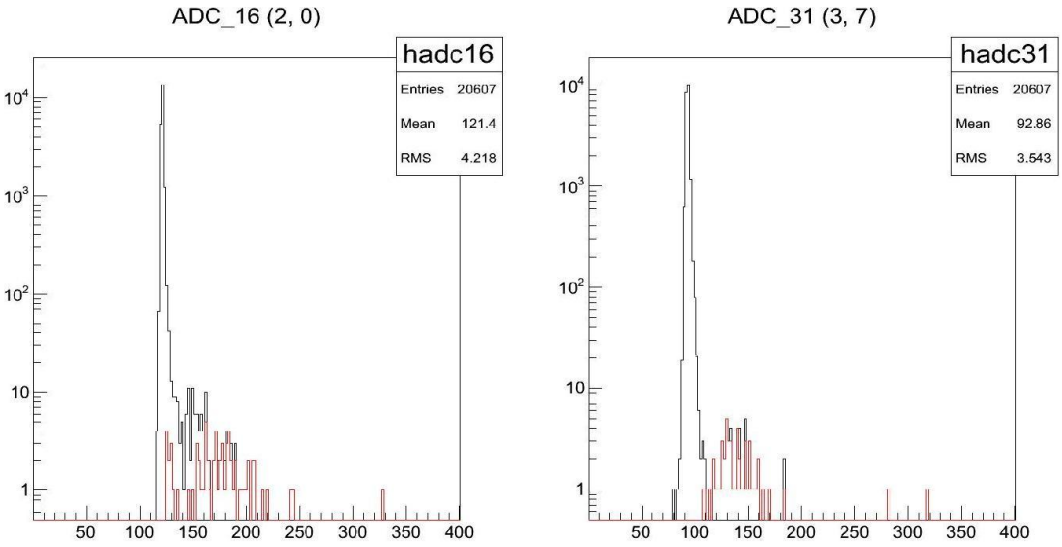

Figure 21: ADC histograms

This data was taken with a smaller prototype detector (Figure 22), which contained an 8x8 array of 3/4" PMT's and a slab of aerogel, in which cosmic rays produced Cherenkov radiation [11]. This TDC-based cutting seems successful in allowing single electron event signal

to be separated from background, so it was determined to be an acceptable DAQ method for the GRINCH detector and prototype. Eventually, in the actual GRINCH detector, only the TDC cluster method will be used to find good events, so that the timing windows, and therefore the background, can be reduced.

Figure 22: Test prototype detector [11]

5 Experiment

5.1 Design and Construction

In the first months of the project, several designs were drawn up and considered for the prototype detector. A top view of the final one that was decided upon is shown in Figure 23, where 1 is the path of a beam incident upon the detector, 2 is a flat vertical 12" x 12" mirror, 3 is the front face of the PMT's, and 4 is the PMT array holder. This cross-sectional geometry was designed to match that of the simulation (Figure 19) and should remain the same for the final GRINCH detector, which will just increase vertically in size. The stipulations for the geometry that are met are that the light/particle beam enter the detector, traverse a length of 70 cm, hit the mirror at an angle of 60 degrees, and then be reflected so that it travel the distance shown before hitting the front face of the PMT's at a right angle. As mentioned earlier, one of the goals for this detector was that the path length of the particle beam in the detector be increased from 40 cm to 70 cm.

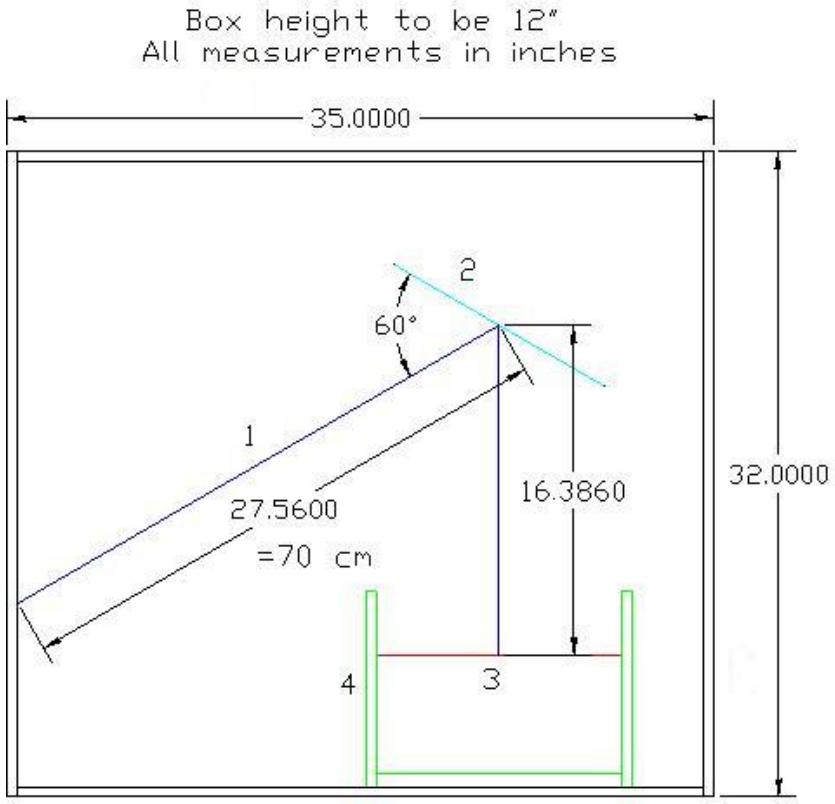

Figure 23: Prototype GRINCH detector design top view

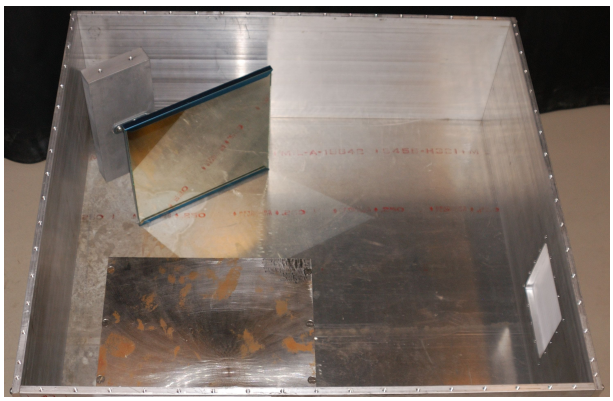

Figure 24: Prototype GRINCH detector bottom view

Next, the construction of the box was completed by the machine shop at William & Mary. As shown in Figure 24 (bottom view), it is made out of aluminum pieces on all sides. The mirror was also purchased and mounted in the box. A laser was then used to aligned the mirror to meet exact specifications. It was then realized that the mirror mounting block was in the path of the electrons traveling though the box. The mirror mounting was redone, as in Figure 25, and a laser was used, yet again, to align the mirror. Additionally, the large PMT array sides

were removed in order to reduce the weight of the prototype detector. The detector was then brought to Jefferson Lab Hall A.

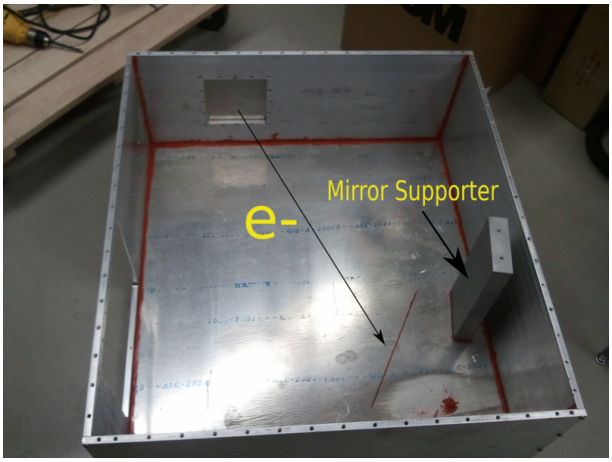

Figure 25: Remounting the mirror [12]

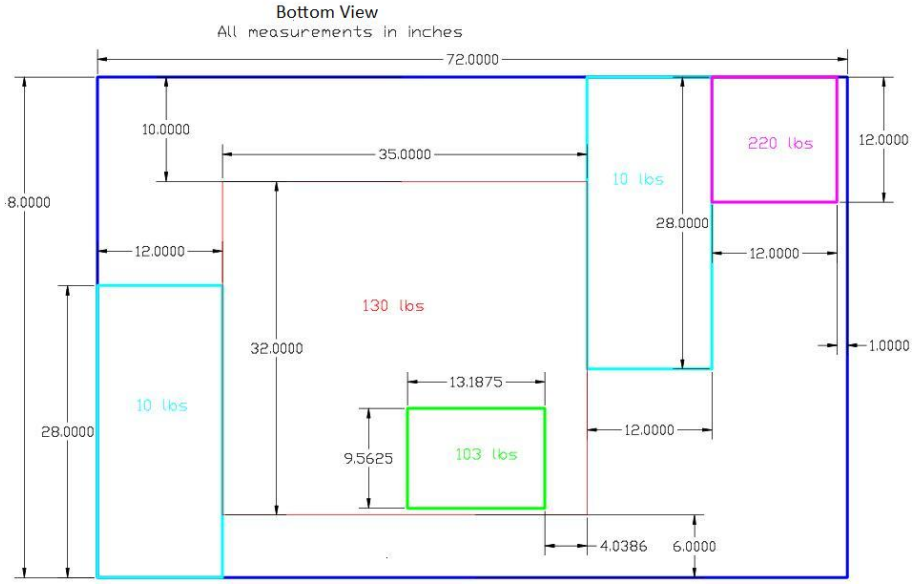

Figure 26: Original mounting platform template

A high voltage distribution system was created for the PMT's. In addition, a design of the weight distribution of the prototype box and surrounding scintillator paddles and lead glass bricks was made (Figure 26) so that a platform could be constructed. This platform was necessary so that the detector could be mounted on a pedestal to "see" the electrons scattering from the target at beam height. Figure 27 shows the platform (somewhat improved upon) and Figure 28 shows it on the pedestal.

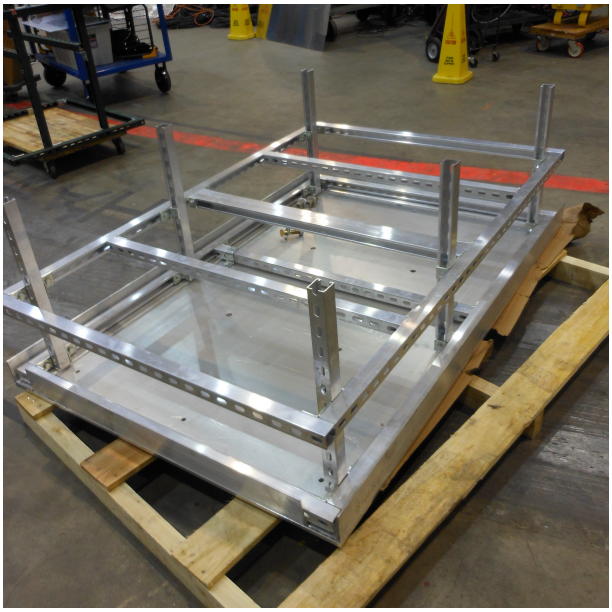

Figure 27: Detector platform

Figure 28: Detector pedestal [12]

5.2 Jefferson Lab Setup

At Jefferson Lab, the cables for the experiment were connected and tested. This took quite a lot of time due to the extensive network of ∼200 cables, for the 81 PMT's, used in the experiment. A cable map is shown in Figure 29. Since the accuracy of the data and results from this experiment is largely based on timing, much effort was taken to measure the time delay of each cable so that the signal going through each bundle of cable would be the same. This was done by using a pocket pulser to send a pulse down one end of a cable. The pulser end of the cable was hooked

up to an oscilloscope, on which the outgoing and reflected pulses could be seen. The timing separation between these two pulses was measured and divided by two to get the time delay. The signal speed in the type of coax cable used, an RG-58, is usually about $0.66c$, so the the following equation was used to double check the time delay:

$$L = vt \tag{19}$$

where L is the cable length, v is the signal speed, and t is the time delay.

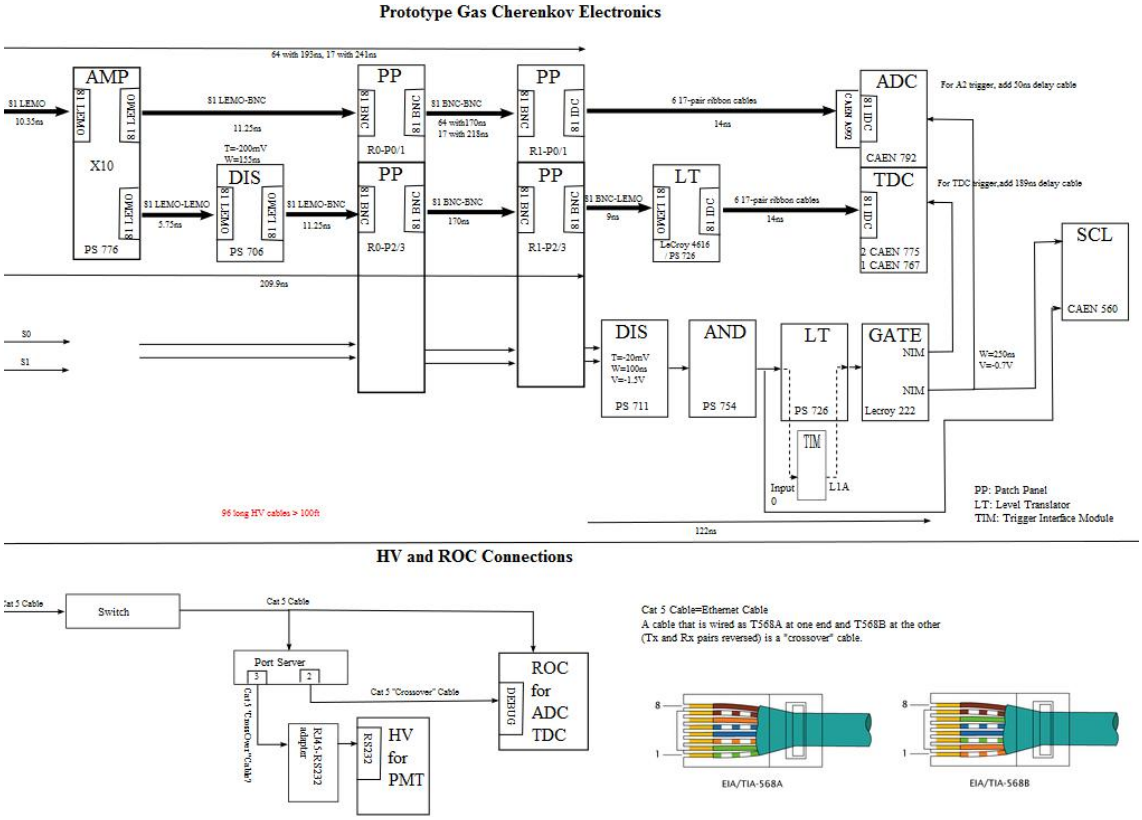

Figure 29: Data acquisition cable map [10]

Next, a stand for supporting the detector during cosmic ray runs was assembled, as shown in Figure 30. Then, the detector box was sealed to prevent air leaks and light leaks - the red sealant in the corners of the box in Figure 31. Figure 32 shows the gas flow valves that were installed for when the detector needs to be pressurized. A blue LED light was installed in the box and tested, as can also be seen in Figure 31. The LED light was put in place for the purpose of gain matching the PMT's. A blue LED was chosen so that the wavelength of the light used to calibrate the PMTs would be as close as possible to that of the light produced by Cherenkov

radiation.

Figure 30: Stand for taking cosmic data [12]

Figure 31: Sealed detector box with LED

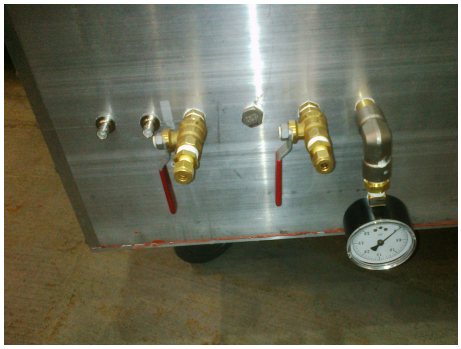

Figure 32: Airflow valves

The box was then completely closed and sealed. After a process of moving the experiment to the other side of Hall A, due to last minute blocking of the target by another experiment,

the prototype detector was set in its cosmic ray stand, and tests were done to check the efficacy of the box's seal. Figure 33 shows the bubbling of Snoop during the test of the pressurized box when an air leak was found. Figure 34 shows the testing for light leaks. Only one light leak was found, and it showed up as an increased PMT count rate, as shown in Figure 35. The air leaks and light leaks were sealed (Figure 36). The PMT's could then be gain matched, which was done by postdoc Huan Yao. Once this process occured, the high voltage connections to the PMT's were reconfigured appropriately, Figure 36.

Figure 33: Snoop air leak test

Figure 34: Testing for light leaks

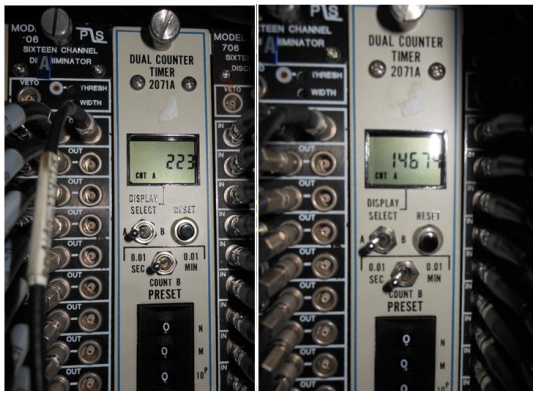

Figure 35: Increase in PMT count rates due to light leak

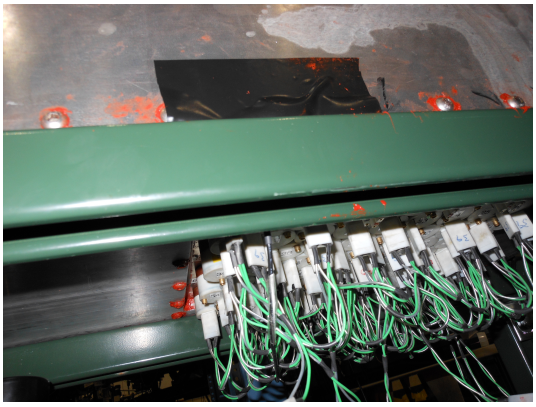

Figure 36: Sealed light leak and high voltage connections

5.3 Data Taking and Results

5.3.1 LED and Cosmics

Before cosmic ray data could be taken, the light from the blue LED in the detector was used by postdoc, Huan Yao, to gain match the PMT's. Since the gain of PMT's is based on the high voltage (Equation 14), the single electron spectrum can be analyzed and the voltage can be adjusted so that all the single electron peaks are around the same channel in the ADC spectrum. The blue LED light is ideal for this task, because it is low intensity and emits light in an appropriate range. Figure 37 shows the ADC data for four PMT's in an LED test. In these histograms, the x-axis is events and the y-axis is an ADC channel number, representing integrated current of the PMT. The pedestal has been subtracted from the plots. The first peaks are the single electron peaks, which at this point were at different channels, so the gain had to

be adjusted to make them the same channel. PMT 4 is a problem PMT, because the gain is too low to get good data.

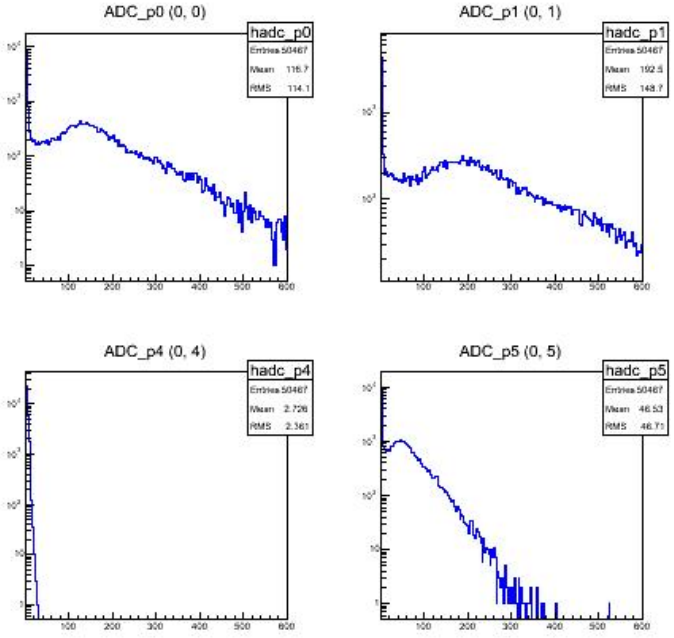

Figure 37: ADC's 0,1,4 and 5 in an LED test

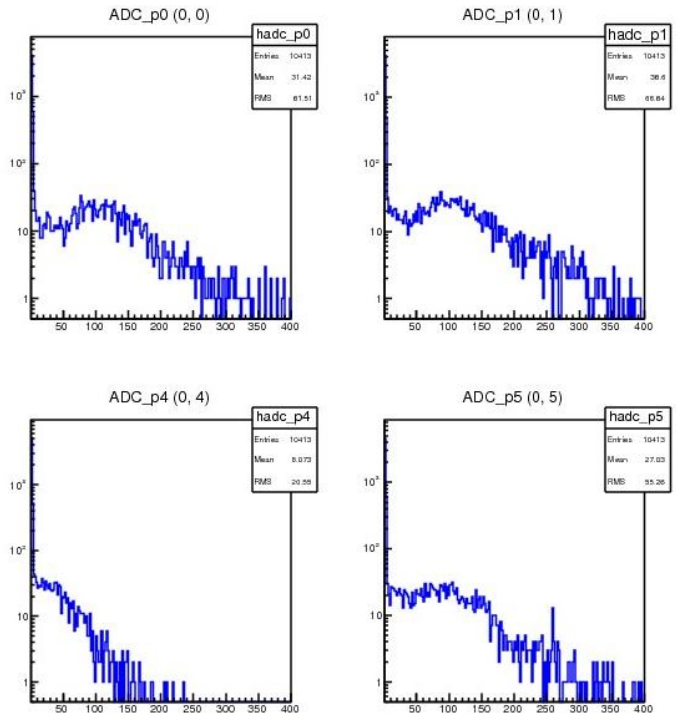

Figure 38: ADC's 0,1,4 and 5 after LED gain matching [12]

Figure 38 shows the same ADC's after gain matching. All single electron peaks have now

been centered as close to channel 100 as possible. However, PMT 4 still has too low gain, even at the maximum high voltage, which should be taken into account in the rest of the data analysis.

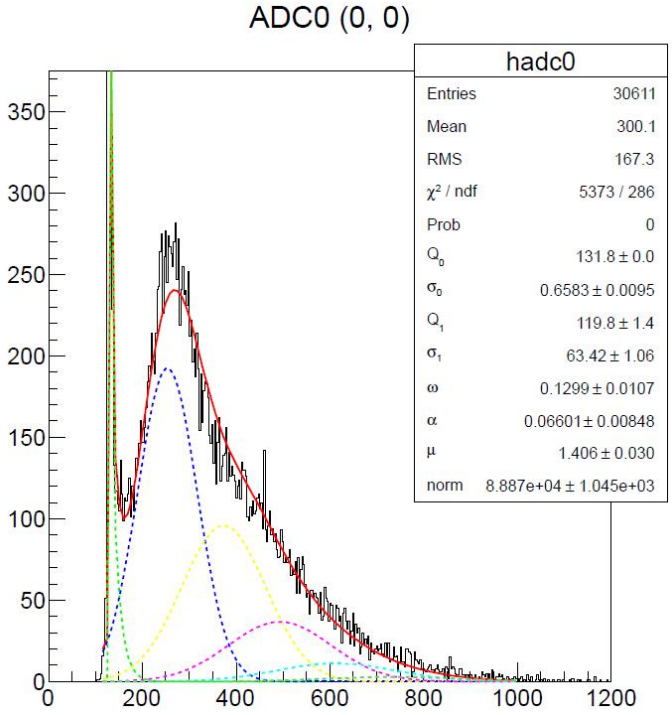

Figure 39: ADC 0 after gain match [10]

Figure 39 shows the ADC 0 data after gain matching, but without the pedestal subtracted. The black is the data and the red curve is the fit curve for the data. The dotted lines are fit lines for the pedestal (green), single electron peak (blue), and multi-electron peaks. The fitting was done by Huan Yao. Q_0 gives the channel number for the pedestal peak and Q_1 gives the channel number for the single electron peak (subtracting Q_0), which is channel 119.8. For this time of ADC, the total integrated charge is 400 pC, divided over 4000 channels. The charge at the single electron peak is calculated with the following equation:

$$Q = 119.8 \text{ channels} \cdot \frac{400 \text{ pC}}{4000 \text{ channels}} = 11.98 \text{ pC} \tag{20}$$

The PMT gain can then be calculated from this:

$$Q = 11.98 \text{ pC} = \text{eN}_\text{e}; \text{N}_\text{e} = 10\text{G} \tag{21}$$

where e is the charge of the electron, N_e is the number of electrons in the cascade, G is the gain, and 10 is amplification of the signal by the amplifier. This gives $N_e = 7.5 \times 10^7$ and $G = 7.5 \times 10^6$, which is reasonable for a PMT with a maximum gain of 10^7.

After the LED tests, some cosmic runs were done. Figure 40 shows the setup. There are scintillators on the top and bottom to trigger the TDC when high energy cosmic ray muons go through, and a layer of aerogel is used for the Cherenkov medium. Figure 41 shows one set of cosmic data for the same four ADC's. This data is used as a detector calibration tool, but there are generally not enough statistics for a proper data analysis.

Figure 40: Setup for cosmic ray data taking [12]

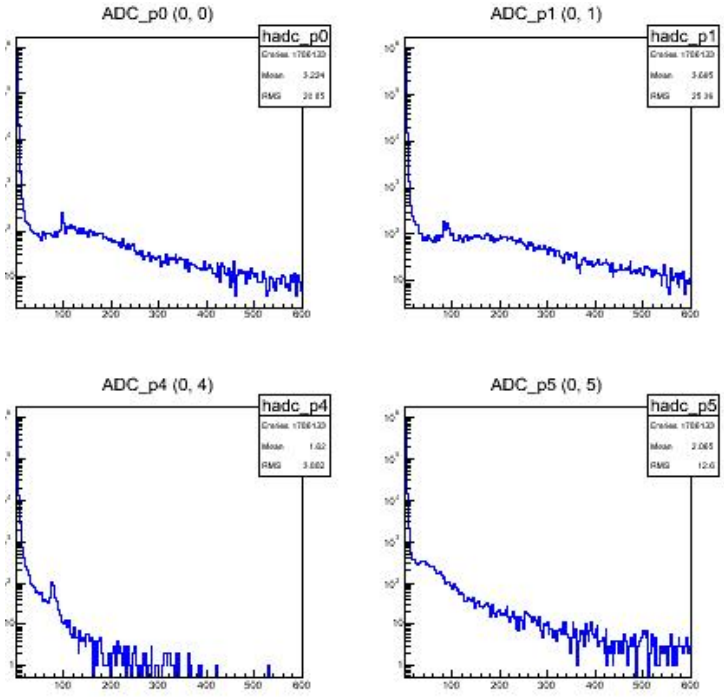

Figure 41: Cosmic data for ADC's 0,1,4 and 5

5.3.2 Beam Data

Next, the prototype GRINCH detector was set up on the pedestal and the electron beam was turned on. Run 2040 is an example of a "good" run, according to the scintillator output. Ideally, ADC signal should overlap (be similarly large) in the two lead glass blocks for a good electron. Figure 42 shows this region. Block 88 is the lead glass block closer to the detector box. Normally, Figure 42 would have only background noise in the bottom left corner and the plot would be zoomed out with the good data in the top right corner. However, as can be seen in Figure 43, the gain in the ADC for PMT 88 is too low. Once fixed, the good data should be more separated from the rest, in the top right corner of the plot.

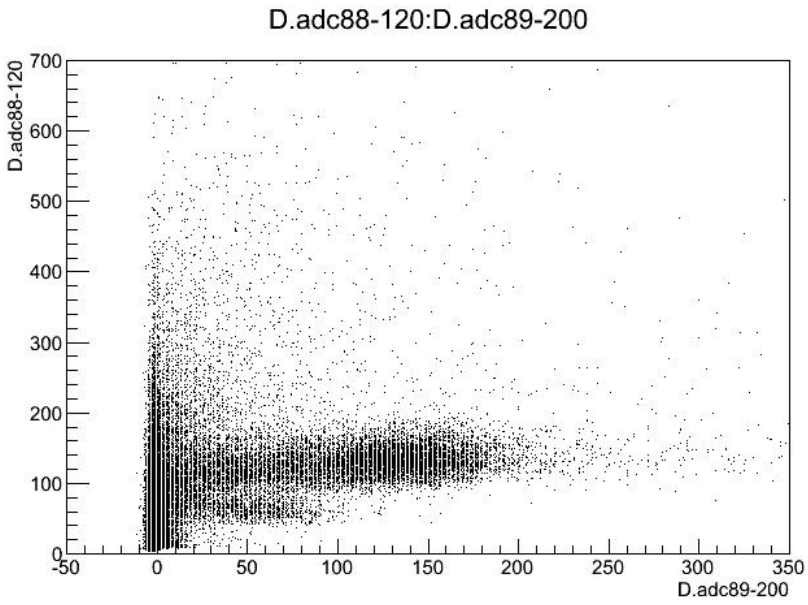

Figure 42: Two dimensional histogram of lead block PMT ADC data

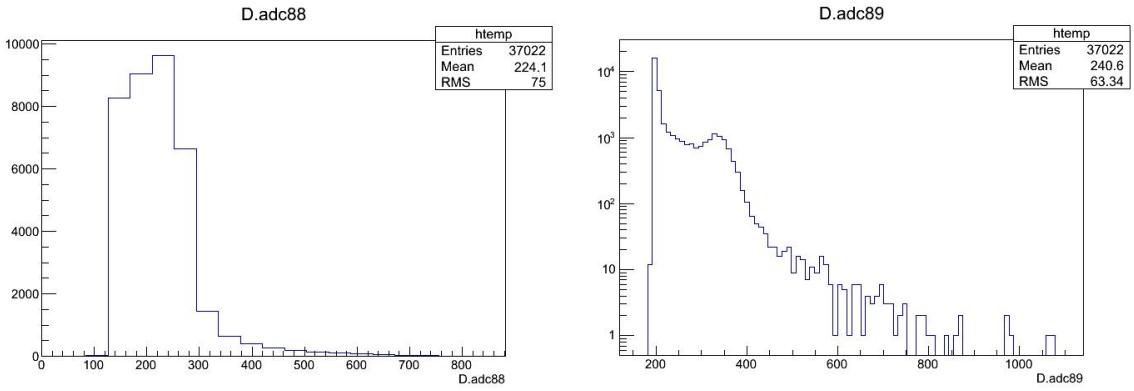

Figure 43: Histogram of lead block PMT ADC data

As can be seen in Figure 43, the pedestal for PMT 88 starts at channel 120 and the pedestal for PMT 89 is 200. If the ADC pedestal data is removed from the two dimensional lead glass ADC plot, then most of the channel 0 ADC 89 data is thrown out, which is desirable. This is shown in the red data in Figure 44. The red data points at channel 0 for ADC 89 likely represent electrons that were stopped in ADC 88.

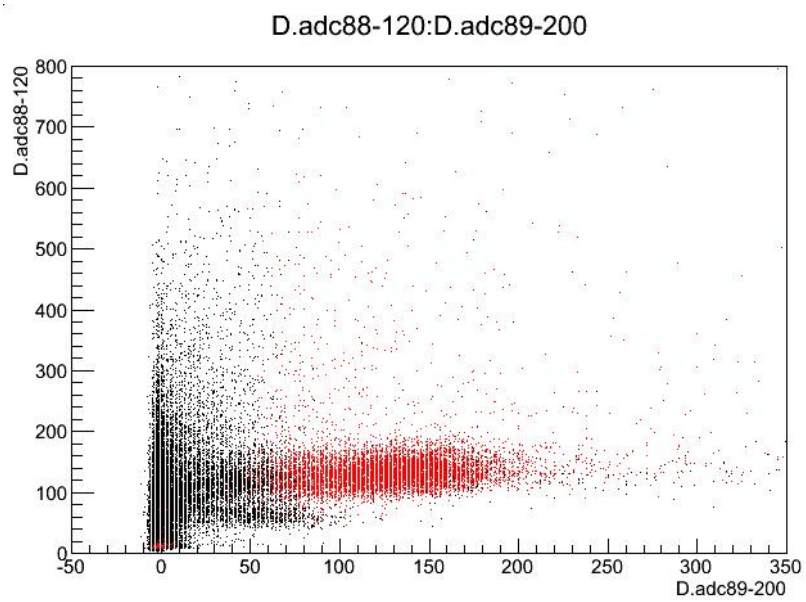

Figure 44: Two dimensional histogram of lead block PMT ADC data after cuts

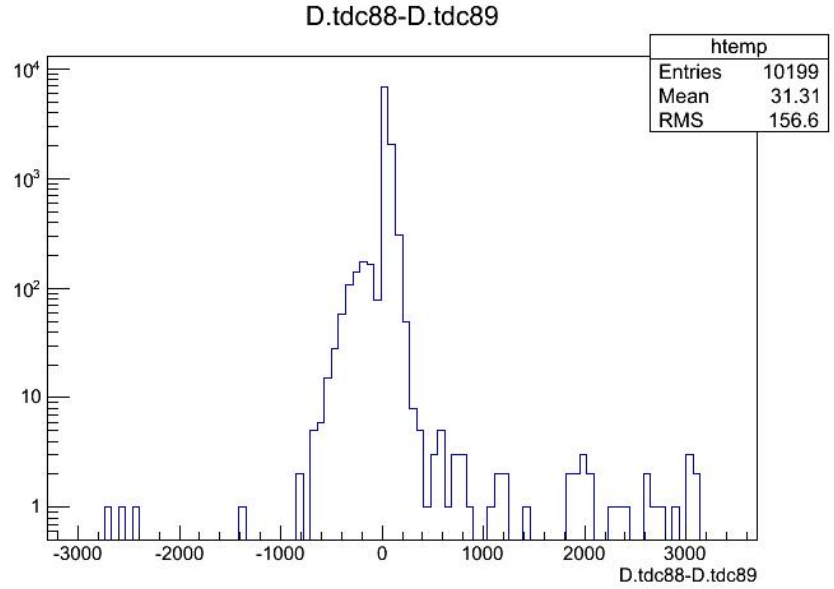

Figure 45: Lead block TDC subtraction data

Another important use for the lead glass block data is to check that the good electron events

are coming through the detector and not from the other direction. The lead glass TDC data can be used for this. The time for these is counted backwards from the trigger, so the TDC time for PMT 89 should come before that of TDC 88. Therefore, the TDC data for PMT 88 subtracted from PMT 89 should be negative (TDC subtraction in Figure 45). Figure **??** shows the original ADC 0 data (from the PMT array) in blue, the PMT 89 - 88 > 0 data removed in red, and this subtraction data and the pedestal (at channel 150) removed in green. More data about the electron beam and target are needed to study the efficiency of this cut.

5.3.3 Beam Data - Lucite

It was determined that the system was not getting enough events with the $C0_2$, so a block of Lucite was placed in the particle path within the detector in order to generate more events. The Lucite was expected to cause a much larger Cherenkov angle due to its index of refraction of 1.5. Therefore, a line of PMT's, the edge of a Cherenkov ring, should fire at once. Figure 46 shows the raw TDC data for one of the PMT's in the main array during a Lucite run. There is an obvious timing peak, but it is noisy.

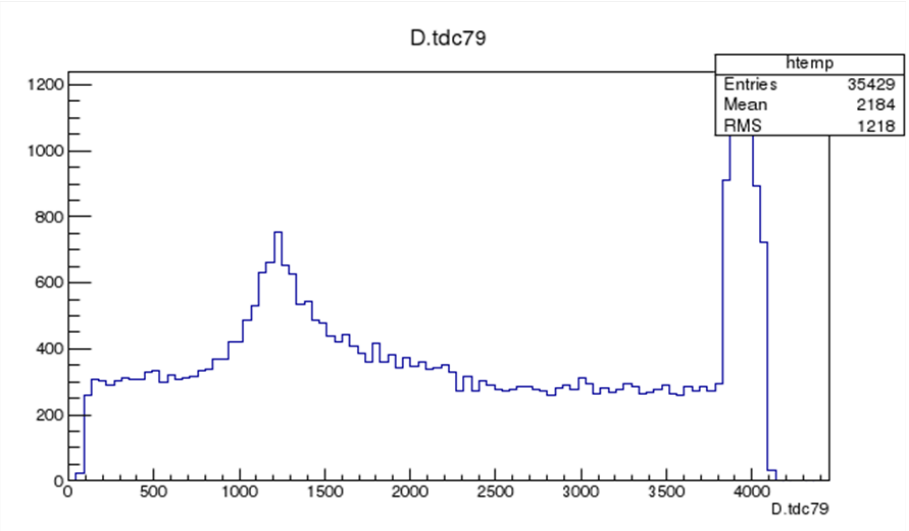

Figure 46: Raw TDC data for PMT 79 (in the main PMT array)

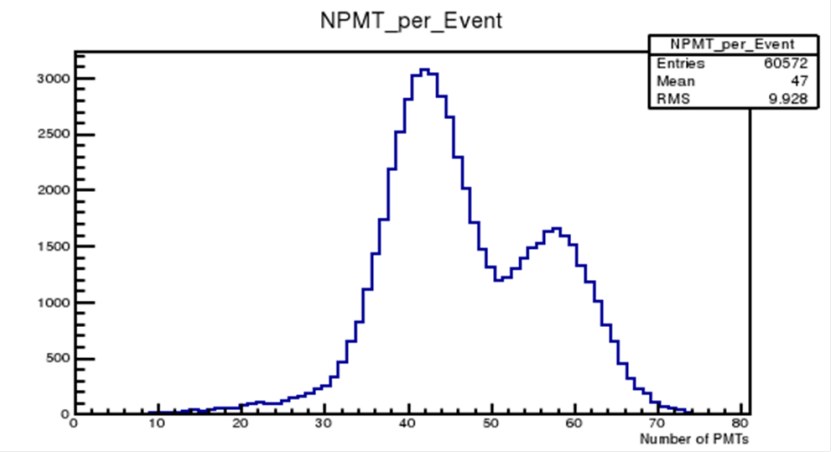

Figure 47: Raw plot of number of PMT's per event

Figure 47 shows the number of PMT's fired per event for the raw data without timing cuts. The data is oddly peaked. When a timing cut (10ns window around TDC peak) is applied (Figure 48), the data is peaked on the lower end of the spectrum for number of PMT's per event. This plot makes more sense, except that ideally there should be more of a peak around 5 or more, because good events require multiple PMT's to fire.

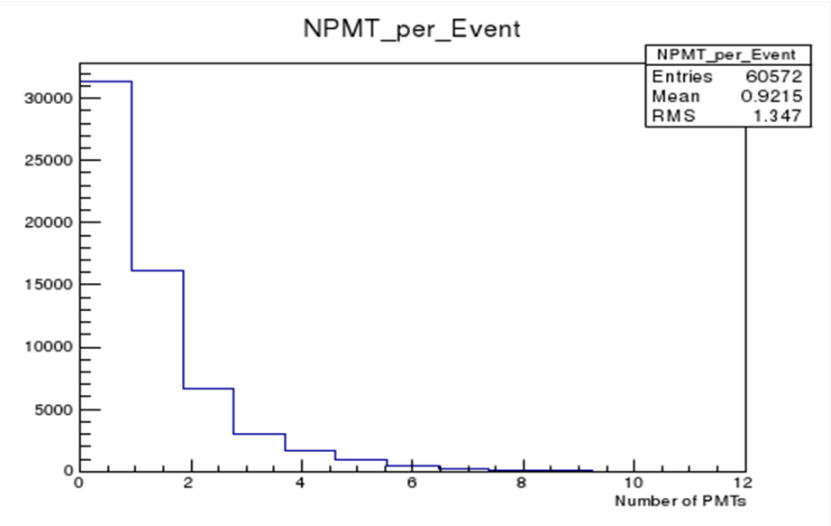

Figure 48: Number of PMT's per event after timing cut

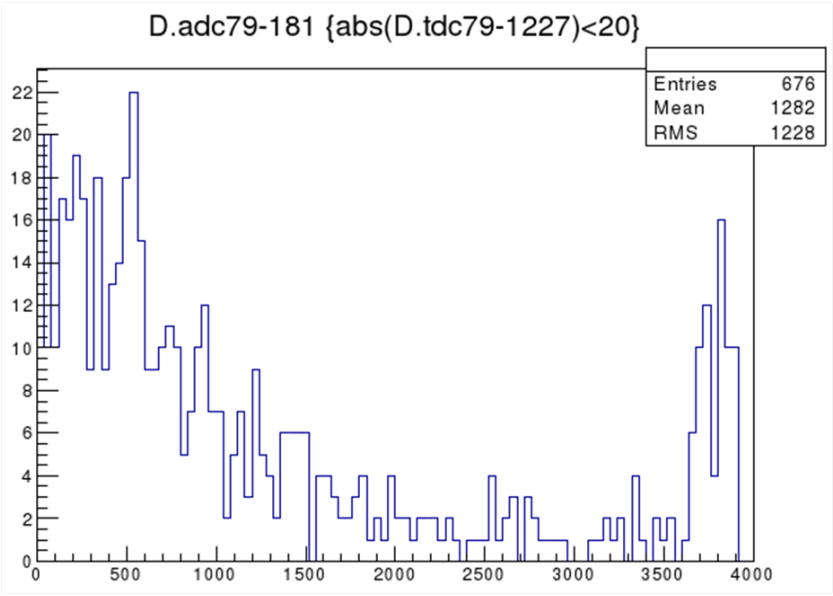

Figure 49: ADC 79 data for 10 ns TDC cut

Figure 49 shows the ADC data, with pedestal subtracted, within the 10 ns timing cut. Figure 50 shows the ADC data, with pedestal subtracted, far outside of the 10 ns timing cut. The fact that they are so similar in shape indicates that much light is flashing in the Lucite and the system cannot separate Cherenkov light from other light. A possible light leak should be investigated.

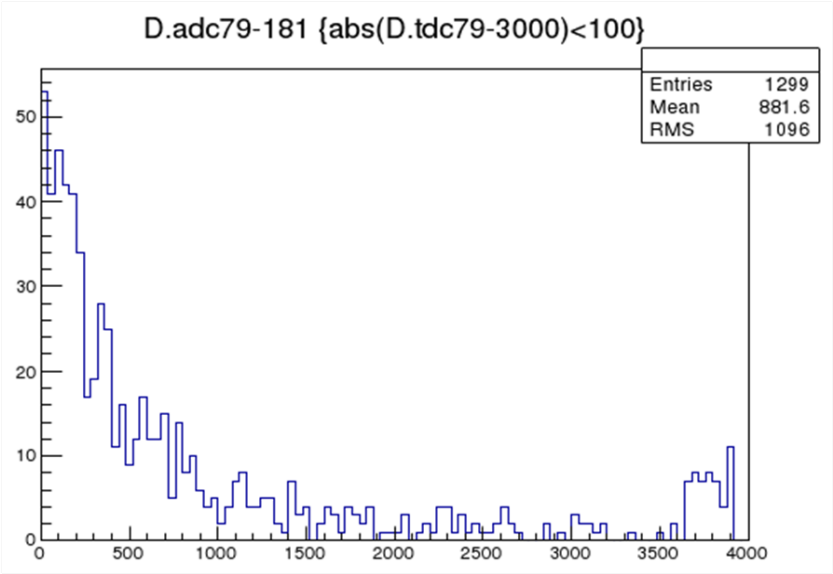

Figure 50: ADC 79 data far outside of 10 ns TDC cut

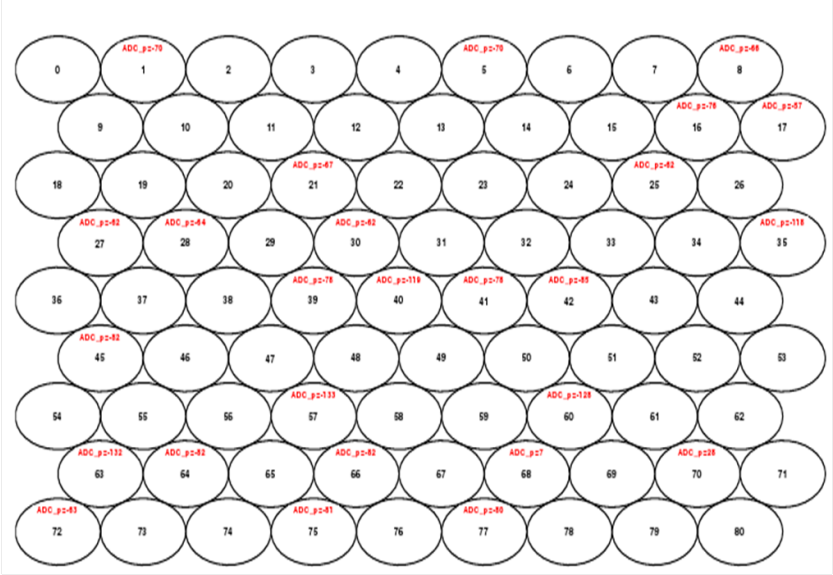

Figure 51: PMT array event display without TDC cut

Figure 51 shows the PMT event display without a TDC cut. The red writing indicates PMT's that fired. As expected from the raw data of number of PMT's per event, (Figure 47), there is a large number of fired PMT's. Figure 52 shows the PMT event display with the 10ns TDC cut and a requirement of at least 8 PMT's fired (for a good event). The system is obviously collecting light, but there is no evidence of Cherenkov rings yet.

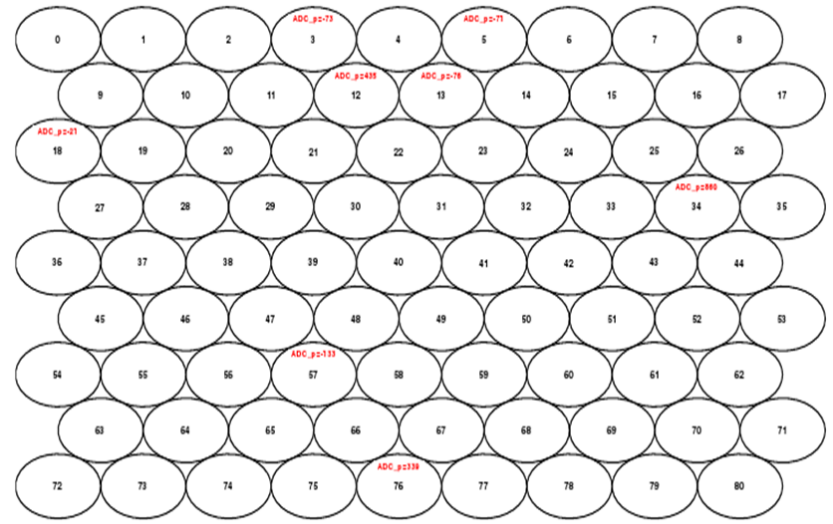

Figure 52: PMT array event display with 10ns TDC cut and number of PMT's $\geq$ 8 cut

6 Conclusions and Future Work

In conclusion, a prototype GRINCH detector to measure electrons scattered off of a polarized Helium-3 target was first designed and created at William and Mary. Then, many steps were taken to install it in Jefferson Lab Hall A. Tests were done to check that all of the cables were working and that it was light-tight and air-tight. The photomultiplier tubes that served to detect the electrons were calibrated with a blue LED light. Then, some cosmic ray data was taken. A small amount of electron beam data was also taken. The integrated current and timing data were both analyzed to look for good events. Some cuts were made on the data from the PMT array using this analysis. However, more data and information are needed to complete the analysis. Lucite was placed in the path of the beam due to too little signal being generated with the $C0_2$. A TDC timing peak was seen, but the data was noisy. The ADC data and PMT event displays indicated that the system was definitely measuring light, so the TDC method seemed effective. However, no Cherenkov rings were successfully separated from other light signals.

In the future, more cosmic and beam taken will be taken. An effort will be made to improve the lead glass block gain. Then, more analysis and cuts will be performed on the TDC and ADC data. The efficiency of these cuts will be reviewed. More data will be taken with the Lucite to get a better understanding of the data produced with it in place. The possibily of a light leak will be investigated. All in all, much positive progress has been made on a useful prototype for the GRINCH detector.

References

[1] T.D. Averett, et al., Proposal: *E12-06-112: Measurement of neutron spin asymmetry A_1^n in the valence quark region using 8.8 GeV and 6.6 GeV beam energies and BigBite spectrometer in Hall A*

[2] G. Franklin et al., Proposal: *(A New Proposal to Jefferson Lab PAC 30) Measurement of neutron spin asymmetry A_1^n in the valence quark region using 8.8 GeV and 6.6 GeV beam energies and BigBite spectrometer in Hall A*, (2006).

[3] T.D. Averett et al., Technical Note: *BigBite Heavy Gas Cherenkov Detector for A_1^n at 6.6 and 8.8 GeV*, (2011).

[4] Bitu, Marinela. Cerenkov Effect. Website - *http://teachers.web.cern.ch/teachers/archiv/hst2002/bubblech/mb* This is an informational page about Cerenkov radiation from the High School Teachers Programme at CERN website.

[5] G.N Afanasiev, *Vavilov-Cherenkov and Synchrotron Radiation: Foundations and Applications*. Dordrecht, The Netherlands: Kluwer Academic Publishers, (2010).

[6] W.R. Leo, *Techniques for Nuclear and Particle Physics Experiments: A How-to Approach*. 2nd Revised. Berlin: Springer-Verlag, (1994).

[7] V.P. Zrelov *Cherenkov Radiation in High Energy Physics: Part I, Cherenkov Radiation in Isotropic and Anisotropic Media: Theory and Experiment Verification*. Jerusalem: Israel Program for Scientific Translations Ltd., (1970).

[8] V.P. Zrelov *Cherenkov Radiation in High Energy Physics: Part II, Cherenkov Counters: Determination of Energy and Directionof Elementary Particles*. Jerusalem: Israel Program for Scientific Translations Ltd., (1970).

[9] J. Engelfried, Ring Imaging Cherenkov Detectors, Instituto de Física, Universidad Autónoma de San Luis Potosí.

[10] BigBite. Website - *http://wm-jlab.physics.wm.edu/mediawiki/index.php/Bigbite_Gas_Cherenkov,* March 2012. This is the main wiki page for the BigBite Cherenkov update.

[11] T.D. Averett, et al., Presentation: *Update on the Gas Ring Imaging Cherenkov (GRINCH) Detector for A_1^n using BigBite*, (2012)

[12] BigBite elog. Website - *http://wm-jlab.physics.wm.edu/phpbb3/viewforum.php?f=4&sid=b502bc7c29e396f51337c5804a2ebbb0,* March 2012. This is the main wiki page for the BigBite elog page.